Volume 10 | Number 43 | 21 November 2019 | Pages 9895–10196

Chemical Science

rsc.li/chemical-science

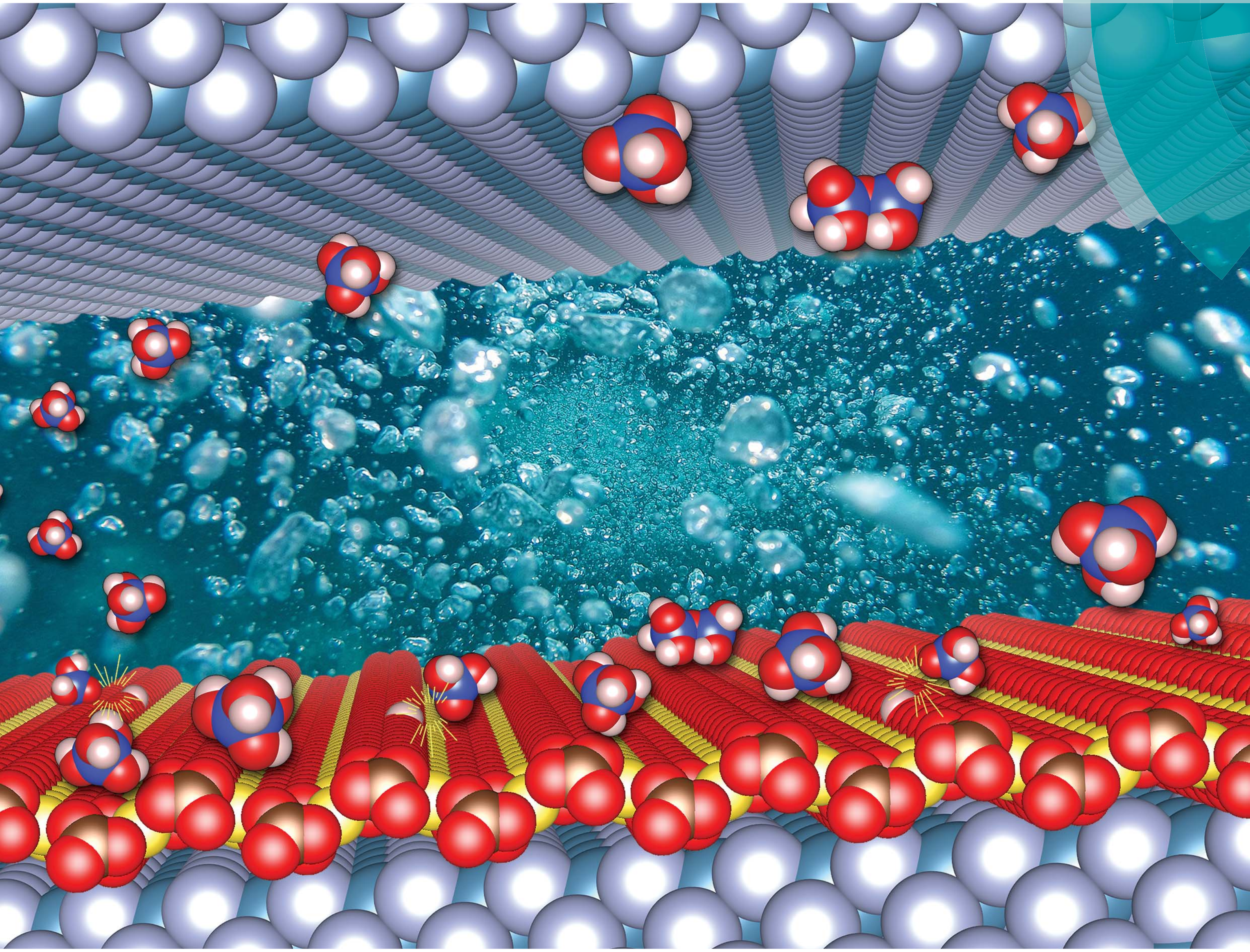

ISSN 2041-6539

ROYAL SOCIETY OF CHEMISTRY | Celebrating IYPT 2019

EDGE ARTICLE

Yann Foucaud, Michaël Badawi, Sébastien Lebègue *et al.*

Synergistic adsorptions of Na_2CO_3 and Na_2SiO_3 on calcium minerals revealed by spectroscopic and *ab initio* molecular dynamics studies

Chemical Science

EDGE ARTICLE

View Article Online
View Journal | View Issue

Check for updates

Cite this: *Chem. Sci.*, 2019, **10**, 9928

All publication charges for this article have been paid for by the Royal Society of Chemistry

Synergistic adsorptions of Na_2CO_3 and Na_2SiO_3 on calcium minerals revealed by spectroscopic and *ab initio* molecular dynamics studies†

Yann Foucaud, *[a] Michaël Badawi, *[b] Lev O. Filippov,[ac] Odile Barres,[a] Inna V. Filippova[ac] and Sébastien Lebègue*[b]

Received 7th July 2019
Accepted 5th October 2019

DOI: 10.1039/c9sc03366a

rsc.li/chemical-science

The synergistic effects between sodium silicate (Na_2SiO_3) and sodium carbonate (Na_2CO_3) adsorbed on mineral surfaces are not yet understood, making it impossible to finely tune their respective amounts in various industrial processes. In order to unravel this phenomenon, diffuse reflectance infrared Fourier transform and X-ray photoelectron spectroscopies were combined with *ab initio* molecular dynamics to investigate the adsorption of Na_2SiO_3 onto bare and carbonated fluorite (CaF_2), an archetypal calcium mineral. Both experimental and theoretical results proved that Na_2CO_3 adsorbs onto CaF_2 with a high affinity and forms a layer of Na_2CO_3 on the surface. Besides, at low Na_2SiO_3 concentration, silica mainly physisorbs in a monomeric protonated form, $Si(OH)_4$, while at larger concentration, significant amounts of polymerised and deprotonated forms are identified. Prior surface carbonation induces an acid–base reaction on the surface, which results in the formation of the basic forms of the monomers and the dimers, *i.e.* $SiO(OH)_3^-$ and $Si_2O_3(OH)_4^{2-}$, even at low coverage. Their adsorption is highly favoured compared to the acid forms, which explains the synergistic effects observed when Na_2SiO_3 is used after Na_2CO_3. The formation of the basic form on the bare surface is observed only by increasing the surface coverage to 100%. Hence, when Na_2CO_3 is used during a separation process, lower Na_2SiO_3 concentrations are needed to obtain the same effect as with lone Na_2SiO_3 in the separation process.

1. Introduction

With an estimated annual worldwide market value of 8.9 billion USD in 2017,[1] alkali silicate reagents are among the most used inorganic reagents worldwide. These environmentally friendly reagents have been intensively studied over past decades[2–6] since they commonly serve as a basis for the production of a large range of silica-containing materials.[7–9] Besides, their interesting properties lead to a wide range of industrial applications as additives, including detergents, foundries, adhesives, surface coatings, and water treatment.[9,10] Alkali silicate glasses, especially sodium silicate (Na_2SiO_3), are also widely used in the froth flotation process, a method based on the adsorption of amphiphilic reagents (collectors) onto mineral surfaces to extract metals from ores. Nowadays, more than 2 billion tons of non-ferrous ores are processed annually by flotation, which has become an unavoidable route to extract metals from rocks, including high-tech and critical metals. Na_2SiO_3 is one of the most common reagents used in the froth flotation process where it plays two key roles, because of its aforementioned properties. First, it increases the efficiency of the flotation process since it prevents slime coating/aggregating by decreasing particle–particle interactions. Second, due to its high affinity for gangue minerals, mostly silicates, it adsorbs onto their surfaces and prevents the adsorption of the collector, keeping the surfaces hydrophilic, *i.e.* depressed. Therefore, Na_2SiO_3 is commonly used in the flotation separation of rare earth minerals,[11] zinc minerals,[12] iron minerals,[13] scheelite ($CaWO_4$),[14–17] fluorite (CaF_2),[18,19] apatite [$Ca_5(PO_4)_3(OH,F)$],[20,21] and many other minerals.

For decades, researchers worldwide have investigated the behaviour of Na_2SiO_3 in aqueous solutions. It is assumed that it dissociates into silica tetrahedra (SiO_4) which can be in SiO_4^{4-}, $SiO_3(OH)^{3-}$, $SiO_2(OH)_2^{2-}$, $SiO(OH)_3^-$, and $Si(OH)_4$ forms depending on the solution pH and the total silica concentration.[22–24] Moreover, some authors demonstrated that silica tetrahedra can polymerise, also depending on the pH, the total silica concentration, and the $SiO_2 : Na_2O$ ratio, a high ratio inducing a high polymerisation degree.[23,25–28] In dilute solutions ($\sim 1 \times 10^{-3}$ mol L^{-1}) and for low to moderate $SiO_2 : Na_2O$ ratio, usually used in flotation, the main species of Na_2SiO_3 are

---

[a] Université de Lorraine, CNRS, GeoRessources Laboratory, F-54000 Nancy, France. E-mail: yann.foucaud@univ-lorraine.fr; michael.badawi@univ-lorraine.fr; sebastien.lebegue@univ-lorraine.fr

[b] Laboratoire de Physique et Chimie Théoriques, Université de Lorraine, UMR 7019 – CNRS, BP239, Boulevard des Aiguillettes, 54 506 Vandoeuvre-lès-Nancy Cedex, France

[c] National University of Science and Technology MISIS, 119049 Moscow, Russia

† Electronic supplementary information (ESI) available. See DOI: 10.1039/c9sc03366a

$Si(OH)_4$ for pH < 9.4, $SiO(OH)_3^-$ for 9.4 < pH < 12.6, and $SiO_2(OH)_2^{2-}$ for pH > 12.6.[29] Also, it is assumed that the polymerisation reaction depends strongly on the $SiO(OH)_3^-$ and $SiO_2(OH)_2^{2-}$ concentrations in solution.[30] To limit operating costs, most flotation processes worldwide are performed at pH 7–11, which means that the silica monomers are dominant, in both $Si(OH)_4$ and $SiO(OH)_3^-$ forms.

Besides, some authors have highlighted strong positive synergistic effects when Na_2SiO_3 is used in flotation pulps where the pH is controlled beforehand by sodium carbonate (Na_2CO_3).[14,15,28,31] In other words, the prior addition of Na_2CO_3 induces a higher efficiency of Na_2SiO_3 in terms of gangue mineral depression, which allows a better flotation selectivity and, hence, higher metal grades in the flotation concentrates. At the moment, although the adsorption of Na_2SiO_3 species has been considerably investigated,[29,32–35] very few studies have been conducted on the Na_2CO_3/Na_2SiO_3 system in flotation[17,28,31,36] and the synergistic effects exhibited by this reagent combination are still poorly understood. Some authors have successfully investigated surface reactivity and synergistic adsorptions/reactions by Fourier transform infrared spectroscopy (FTIR),[37–40] by X-ray photoelectron spectroscopy (XPS),[41–43] and by *ab initio* molecular dynamics (AIMD)[37,44–46] with couplings between the above-mentioned techniques. In the present study, we use a combination of diffuse reflectance infrared Fourier transform spectroscopy (DRIFTS), XPS, and AIMD simulations to gain an understanding of the molecular mechanisms involved in the Na_2SiO_3 adsorption onto bare surfaces and onto surfaces prior treated with Na_2CO_3. Fluorite (CaF_2), a simple cubic calcium-bearing mineral, was chosen for this study since it is considered as an archetype of minerals that can be depressed by Na_2SiO_3.

2. Materials and methods

2.1. Materials

The spectroscopic studies were conducted with pure CaF_2 mineral acquired from Mexico. Chemical analyses were carried out using inductively coupled plasma-atomic emission spectrometry (ICP-AES) for major elements and ion-sensitive electrode (ISE) for fluorine (Table 1). Fluorite was of satisfactory purity although 1.26% Si was present, indicating contamination by quartz. The pure mineral was crushed in an agate mortar and dry sieved to obtain a −40+20 μm size fraction. All the reagents used (Na_2SiO_3, Na_2CO_3, and NaOH) were supplied by Aldrich and were of technical quality.

2.2. Spectroscopic studies

Each test was conducted with 0.5 g of −40+20 μm fraction of pure CaF_2. For the control sample, *i.e.* without the addition of any reagent, CaF_2 was treated in 5 mL of deionised water (R = 18.2 MΩ cm) at pH 10 during 15 min. For the other tests, each reagent (Na_2CO_3 and Na_2SiO_3) was prepared in aqueous solution with deionised water at pH 10, prior to the conditioning stage. When the reagents were used alone, the mineral was treated in 5 mL of the reagent solution during 15 min. After the conditioning stage, the sample was filtered using ashless filter paper and rinsed three times with deionised water. When the reagents were used in combination, they were added sequentially: the mineral was first conditioned in 5 mL of Na_2CO_3 solution during 15 min and the conditioning solution was eliminated. Then, the sample was washed three times with deionised water and conditioned with 5 mL of Na_2SiO_3 solution during 15 min. The same solid/liquid separation and washing procedure was applied at the end of the conditioning stage. The pH was adjusted to 10 for solution preparation and during the conditioning stage by adding 0.1 M NaOH or HCl solution. Since Na^+ and Cl^- are assumed to not adsorb on mineral surfaces, they are eventually located in the electrical double layer from which they are likely to be eliminated during the washing procedure. In the reference sample (pure CaF_2), neither Na^+ nor Cl^- ions were detected by XPS analyses, which substantiates the previous assumption.

FTIR analyses were conducted with the diffuse reflectance method to maximise the surface signal. The spectra were recorded using a Bruker IFS 55 spectrometer equipped with a large-band mercury-cadmium-telluride (MCT) liquid-nitrogen-cooled detector and associated with a diffuse reflectance attachment (Harrick Corporation). The FTIR spectra were acquired in the mid-infrared range between 4000 cm^{-1} and 600 cm^{-1} with a spectral resolution of 2 cm^{-1}. Dry mineral samples were analysed without dilution in potassium bromide (KBr), used as a reference.

The XPS spectra were acquired using an X-ray photoelectron spectrometer, a Kratos Axis Ultra DLD, equipped with a monochromatic Al Kα X-ray source (1486.7 eV) operated at 120 W (8 mA and 15 kV). The wide-scan spectra were recorded with a resolution of 1.0 eV and a pass energy of 160 eV while the high-resolution spectra were acquired with a resolution of 0.1 eV and a pass energy of 20 eV. For carbon and oxygen, the resolution was decreased to 0.05 eV. The hybrid mode was employed, using a magnetic-electrostatic lens and a charge neutraliser since the samples were not conducting. After the acquisition, the adventitious carbon was used as a reference with the C–C bond binding energy set at 284.6 eV. Vision 2.2.10 software, supplied by Kratos Analytical (Manchester, UK), was employed to process the data.

2.3. AIMD simulations

For AIMD simulations, a primitive cubic cell of CaF_2 was generated and fully relaxed to obtain lattice parameters $a = b = c = 5.46$ Å. Then, a (111) surface was created from the relaxed

Table 1 Major element amounts in pure CaF_2 used in this study (ICP-AES and ISE)

Ca (%)	P (%)	Si (%)	Mg (%)	Al (%)	Fe (%)	Na (%)	K (%)	Ti (%)	Mn (%)	F (%)	LOI (%)	Total (%)
50.06	<LOD	1.26	<LOD	0.03	<LOD	<LOD	<LOD	<LOD	<LOD	44.59	2.36	98.30

bulk since the (111) cleavage plane represents the most exposed surface for CaF_2.[47–49] A supercell containing 72 atoms (24 Ca and 48 F) was obtained, which is constituted of 2 layers of calcium atoms and 4 layers of fluorine atoms including one plane of 12 seven-coordinated calcium atoms on the (111) surface. To avoid any unwanted interaction due to the periodicity of the cell, a vacuum of 10 Å was set between the uppermost atom, including the added molecules, and the upper limit of the cell following the *z* axis. For all the calculations, 3 layers of bottom atoms in the cell (1 layer of calcium atoms and 2 layers of fluorine atoms) were frozen to their bulk positions.

The structure and total energy of the systems were determined by density functional theory calculations,[50,51] using the Vienna *ab initio* simulation program (VASP).[52] The semilocal Perdew–Burke–Ernzerhof (PBE) exchange-correlation functional proposed by Perdew and co-workers[53] was employed, in the generalized gradient approximation (GGA). The projector-augmented wave (PAW) method[54,55] was used to describe the electron–ion interactions with a plane wave cutoff of 300 eV and the Kohn–Sham equations[51] were solved self-consistently[56] until the energy difference between the cycles became lower than 10^{-5} eV. A Methfessel and Paxton smearing[57] of $\sigma = 0.1$ eV was employed to help the total energy convergence. Due to the large size of the cell, all the calculations were performed using the Γ-point only. Structural relaxations were realised until all the forces were smaller than 0.05 eV A^{-1}. The D2 correction of Grimme[58] was used to include van der Waals forces. A Nosé–Hoover thermostat was used and the temperature was set to 300 K. The time step was 1 fs and, to reach a total simulation time of 100 ps, 100 000 steps were realized.

The internal adsorption energies of species on the (111) fluorite surface were calculated based on the average energy of each system computed for the last 90 ps of the simulation, to exclude a 10 ps thermalisation period. The total internal adsorption energy was calculated as the difference between the energy of the surface with the adsorbed molecule(s) and the sum of the energies of the non-adsorbed surface and the isolated molecule(s). The energies of those systems systematically correspond to optimised geometries since they were calculated in AIMD simulations, either when the molecule is isolated or when it is adsorbed. The dispersion contribution to the total adsorption energy was calculated in a similar way by considering the dispersion contribution only.

3. Results

3.1. Adsorption of each of Na_2CO_3 and Na_2SiO_3 alone on CaF_2

3.1.1. Carbonation of CaF_2 by the presence of Na_2CO_3. The DRIFT spectrum of CaF_2 treated with 5×10^{-2} mol L^{-1} of Na_2CO_3 displayed bands at 2492, 1775, 1650, 1439, 879, and 842 cm^{-1} that were not present in the spectrum of CaF_2 conditioned in water only (Fig. 1a). The bands located at 2492, 1775, 1439, and 879 cm^{-1} were ascribed to CO_3^{2-} in either Na_2CO_3 or $CaCO_3$,[59] which could not be distinguished from each other. The band at 842 cm^{-1} was attributed to $NaHCO_3$ as well as the band located at 1650 cm^{-1}, which overlapped the band corresponding to water molecules, around 1620–1640 cm^{-1} for CaF_2 conditioned in water. Considering the low intensity of the band at 842 cm^{-1}, $NaHCO_3$ was in a minority in the adsorbed layer compared to $CaCO_3$ and/or Na_2CO_3. However, at pH 10, HCO_3^- is present in the same amount as CO_3^{2-} in solution since the pK_a of HCO_3^-/CO_3^{2-} is 10.2. Hence, it could be assumed that CO_3^{2-} was more likely to adsorb on the CaF_2 surface than HCO_3^-. Overall, the DRIFT results did not permit a determination of the nature of the carbonate layer formed on the CaF_2 surface, considering the significant amounts of both Na^+ and Ca^{2+} available in solution. Indeed, some authors demonstrated that the CaF_2 dissolution rate is significant, which implies that the thermodynamic equilibrium is reached in only one hour.[60] Considering a solubility product of 7×10^{-11} for CaF_2,[61] the amount of Ca^{2+} ions available in solution was high enough to form a $CaCO_3$ layer on the surface. However, it could be assumed that the formation of the carbonate layer was quite fast and could prevent mineral dissolution.

To confirm the previous conclusions and to gain an understanding of the molecular mechanisms involved in the CaF_2 surface carbonation, XPS analyses were performed on CaF_2 conditioned in deionised water, in a 5×10^{-2} mol L^{-1} Na_2CO_3 solution, and in a 5×10^{-3} mol L^{-1} Na_2CO_3 solution, at pH 10. First, for CaF_2 conditioned in deionised water, calcium, fluorine, and oxygen were identified (Table S1 in ESI†) along with contaminant elements such as C, corresponding to adventitious carbon, and Si (3.0 at%), the presence of which had been previously highlighted by chemical analyses (Table 1). The O(1s) spectrum exhibited two components with binding energies of 532.1 eV (11.1 at%) and 533.2 eV (3.4 at%) that were attributed to adsorbed carbonate and water molecules, respectively (Fig. S1 in ESI†), which was in accordance with the DRIFT spectrum of pure CaF_2 (Fig. 1a). Besides, the F/Ca atomic ratio of 1.73 indicated that the surface was depleted in terms of fluorine atoms since the theoretical F/Ca ratio should be 2 (Table S2 in ESI†). This could be attributed to the fact that the (111) surface, which is the main cleavage plane for fluorite,[45–47] exhibits seven-coordinated calcium atoms while they are eight-coordinated in the fluorite crystal.[49,63,64] This under-coordination means that the first atomic layer is constituted of only 7 fluorine atoms along with 2 calcium atoms, which results in a surface F/Ca ratio of 1.75, in agreement with the ratio measured here. Overall, no hydroxyl groups as well as no sodium atoms were identified on pure CaF_2, indicating that the fluorite surface was not hydroxylated at pH 10.

The two different Na_2CO_3 concentrations led to similar trends for XPS that were, consistently, more pronounced for 5×10^{-2} mol L^{-1}. The following discussion will thus focus on results for the highest concentration. First, sodium atoms were identified (4.5 at%) with a Na(1s) binding energy of around 1071.5 eV (Fig. 1b): this corresponded to an intermediate value between Na–O bonds of Na_2CO_3 species[62] and Na–F bonds of NaF or Na–O bonds of $NaHCO_3$, the binding energy of which is known to be lower. However, DRIFTS results demonstrated the absence of $NaHCO_3$ (Fig. 1a), which means that the binding energy of 1071.5 eV corresponds to an intermediate value

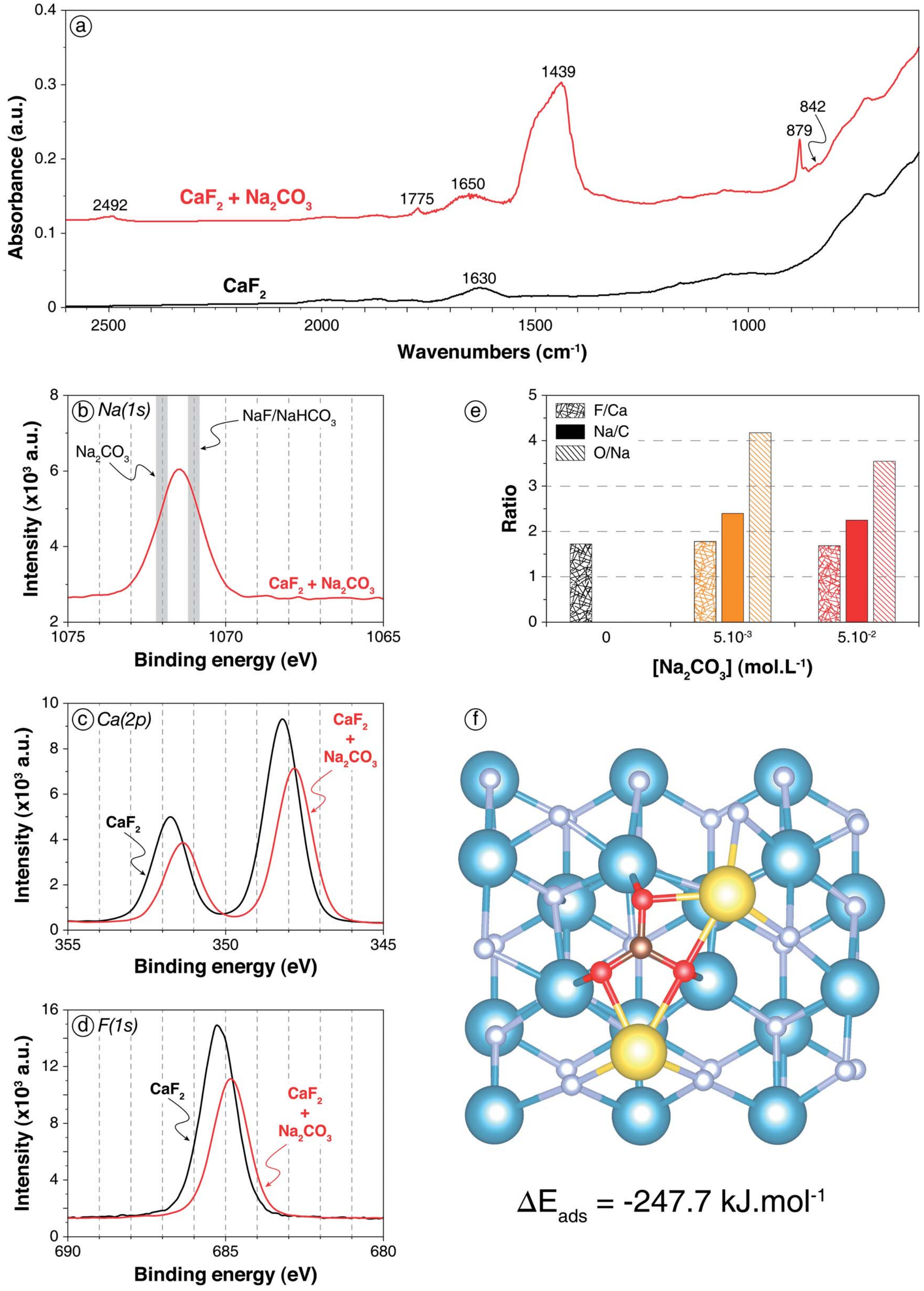

Fig. 1 Carbonation of CaF_2 surface by Na_2CO_3 addition. (a) Infrared spectra of CaF_2 conditioned in deionised water (black) and in a 5×10^{-2} mol L^{-1} Na_2CO_3 solution (red). (b) XPS Na(1s) spectrum of the sample conditioned in a 5×10^{-2} mol L^{-1} Na_2CO_3 solution, with the common binding energies of Na–O and Na–F bonds (from Moulder[62]). (c) XPS Ca(2p) spectra of the sample conditioned in water and of the sample conditioned in a 5×10^{-2} mol L^{-1} Na_2CO_3 solution. (d) XPS F(1s) spectra of the sample conditioned in water and of the sample conditioned in a 5×10^{-2} mol L^{-1} Na_2CO_3 solution. (e) F/Ca, Na/C, and O/Na ratios of CaF_2 conditioned in deionised water (black), in a 5×10^{-3} mol L^{-1} Na_2CO_3 solution (orange), and in a 5×10^{-2} mol L^{-1} Na_2CO_3 solution (red). The ratios were calculated with the corresponding component (C–O from CO_3) for O and C. (f) Snapshot of a top view of the (111) CaF_2 surface with a Na_2CO_3 molecule adsorbed onto the surface after 35 ps of AIMD simulation. The blue, grey, red, maroon, and yellow spheres represent the calcium, fluorine, oxygen, carbon, and sodium atoms, respectively.

between Na–O bonds of Na_2CO_3 and Na–F bonds. Besides, the $Ca(2p_{3/2})$ and $Ca(2p_{1/2})$ binding energies were shifted from 348.2 eV and 351.8 eV for pure CaF_2 to 347.8 eV and 351.3 eV, respectively, for CaF_2 + Na_2CO_3 (Fig. 1c). This shift was attributed to the presence of Ca–O bonds that have lower binding energies than Ca–F bonds.[62] Moreover, the F(1s) binding energy was shifted from 685.2 eV for pure CaF_2 to 684.8 eV for CaF_2 + Na_2CO_3 (Fig. 1d), demonstrating the existence of the aforementioned F–Na bonds, along with F–Ca bonds.[62] The O(1s) spectrum presented two components with binding energies of 531.7 eV (15.9 at%) and 533.6 eV (0.8 at%) for 5×10^{-2} mol L^{-1} Na_2CO_3 (Table S1 and Fig. S1 in ESI†). The first one was attributed to C–O bond of Na_2CO_3,[62] while the second one could be ascribed to C–O bond of $NaHCO_3$, which was present in very small amounts as the DRIFTS results demonstrated (Fig. 1a). However, the second component, with a binding energy of 533.6 eV, exhibited in the O(1s) spectrum for 5×10^{-2} mol L^{-1} Na_2CO_3 was absent for 5×10^{-3} mol L^{-1} Na_2CO_3. This demonstrated that the CO_3^{2-} ions were more likely to adsorb onto CaF_2 since, at low Na_2CO_3 concentration, no HCO_3^- species were identified on the surface. Besides, the F/Ca ratio was not significantly affected by the addition of Na_2CO_3 (Fig. 1e) regardless of the concentration. The Na/CO_3 ratio was 2.40 at low Na_2CO_3 concentration and 2.25 at high Na_2CO_3 concentration, indicating that the layer formed on the surface was Na_2CO_3 with an excess of Na^+, probably adsorbed along with HO^- ions, which however decreased when Na_2CO_3 concentration was increased. Overall, Na_2CO_3 adsorbed onto CaF_2 mostly in Na_2CO_3 form (Fig. 1e), establishing Ca–O and Na–F bonds with the surface atoms (Fig. 1b–d). Small amounts of $NaHCO_3$ were exhibited at high Na_2CO_3 concentration, which was in accordance with the DRIFTS results (Fig. 1a).

AIMD simulations confirmed that, when a Na_2CO_3 molecule was set onto the CaF_2 (111) surface, it adsorbed with each oxygen atom establishing an O–Ca bond with a different calcium atom (Fig. 1f). Their average lengths for the whole simulation were 2.36, 2.36, and 2.43 Å with a standard deviation of around 0.10 Å. Each sodium atom established two Na–F bonds with surface fluorine atoms with $d_{Na-F1} = 2.41$ Å and $d_{Na-F2} = 2.45$ Å (Fig. 1f). Also, each sodium atom was bonded to two oxygen atoms of the CO_3^{2-} ion with $d_{Na-O1} = d_{Na-O2} = 2.35$ Å on average. The Na_2CO_3 molecule adsorbed with $\Delta E_{ads} = -247.7$ kJ mol^{-1} including $\Delta E_{disp} = -91.3$ kJ mol^{-1}, which indicated a highly favoured adsorption as well as high induced dipole-induced dipole forces. This theoretical result was in agreement with both DRIFTS and XPS results that allowed identification of carbonate and Ca–O/Na–F bonds on the surface, respectively.

3.1.2. Adsorption of Na_2SiO_3 on CaF_2 bare surface. Compared to CaF_2 treated in deionised water only, CaF_2 treated in a 5×10^{-2} mol L^{-1} Na_2SiO_3 solution exhibited two weak broad bands in the DRIFT spectrum at 1510 and 1405 cm^{-1} (Fig. 2a), which probably corresponded to surface carbonation (HCO_3^- and CO_3^{2-}, respectively). Moreover, a broad band between 1200 and 900 cm^{-1} with a maximum at 1080 cm^{-1} was present (Fig. 2a), which could be attributed to the Si–O asymmetric stretching vibration. Some authors demonstrated that the Si–O asymmetric stretching vibration wavenumber in silica is affected by the proportion of non-bonding oxygen atoms.[22,23,65,66] Monomers exhibit wavenumbers around 850 cm^{-1} while highly polymerised silica can display wavenumbers as high as 1300 cm^{-1} for the Si–O asymmetric stretching vibration.[23,65,66] Moreover, the proportion of H^+ or Na^+ ions bonded to the terminal oxygen atoms, which depends on the pH and the Si/Na ratio, is also known to shift the wavenumbers of this vibration.[22] Based on the literature, the broad band between 1200 and 900 cm^{-1} was difficult to interpret: it could be attributed either to moderately polymerised adsorbed silica or to free silica monomers adsorbed in basic form, *i.e.* $SiO(OH)_3^-$. Furthermore, the adsorption of the silica tetrahedra on the surface, regardless of their form, probably shifts the wavenumbers of the Si–O asymmetric stretching vibration.

For low Na_2SiO_3 concentration (5×10^{-3} mol L^{-1}), small amounts of sodium atoms (0.84 at%) along with silica atoms (5.7 at% compared to 3.0 at% for pure CaF_2) were identified by XPS (Table S1 in ESI†), indicating the adsorption of Na_2SiO_3 onto CaF_2. The Na(1s) binding energy was 1071.9 eV, which mostly corresponded to Na–O bonds (Fig. 2b). Hence, it could be considered that the adsorbed Na atoms were mainly bonded to silica tetrahedra in anionic form. Moreover, the F(1s) as well as the Ca(2p) binding energies were not affected by the adsorption of Na_2SiO_3 at low concentration (Fig. 2c and d), indicating a physisorption of silica tetrahedra onto the CaF_2 surface. The Si(2p) spectrum exhibited two main components (Fig. 2e) at 102.1 eV (1.2 at%) and 103.2 eV (4.5 at%), which could be attributed to Si–O bonds and Si–O–Si bonds, respectively.[67–69] The low-energy component (102.1 eV) could be ascribed to a Si–O bond in which the oxygen atom is either partly charged ($Si–O^-$) or stabilised by a sodium atom (Si–O–Na) or a calcium atom (Si–O–Ca), as Na and Ca exhibit lower electronegativity than Si,[70] inducing lower Si(2p) binding energy. Furthermore, the high-energy component (103.2 eV) could also be related to Si–O–H bonds since H and Si display similar electronegativity.[70] Overall, the Si(2p) spectrum was difficult to interpret considering the influence of chemical environment on binding energies, since the chemical environment of the oxygen atom ($Si–O^-$, Si–O–H, Si–O–Na, Si–O–Ca, and Si–O–Si) affects significantly the Si(2p) binding energies. The F/Ca ratio was not affected by the Na_2SiO_3 adsorption at low concentration, indicating no chemical modification of the surface (Fig. 2f). Moreover, the O/Si ratio was 3.61 and the O/Na ratio was 24.35 (Fig. 2f), which corresponded to an overall formula of $Si_{6.75}O_{24.35}NaH_{20.70}$, very close to $Si(OH)_4$. Hence, at low Na_2SiO_3 concentrations, the silica was mostly in monomeric protonated form, *i.e.* $Si(OH)_4$.

At high Na_2SiO_3 concentration, sodium (4.2 at%) and silica (16.1 at%) were also identified on the surface (Table S1 in ESI†). No significant changes in Na(1s) and F(1s) binding energies were observed compared to low Na_2SiO_3 concentration (Fig. 2b and c). However, the $Ca(2p_{3/2})$ and $Ca(2p_{1/2})$ binding energies were shifted from 348.2 eV and 351.8 eV for pure CaF_2 to 348.0 eV and 351.5 eV, respectively (Fig. 2d). Though of low significance, it could correspond to the formation of Ca–O bonds. The Si(2p) spectrum exhibited only a component at 103.2 eV (Fig. 2e) that was ascribed to polymerised silica

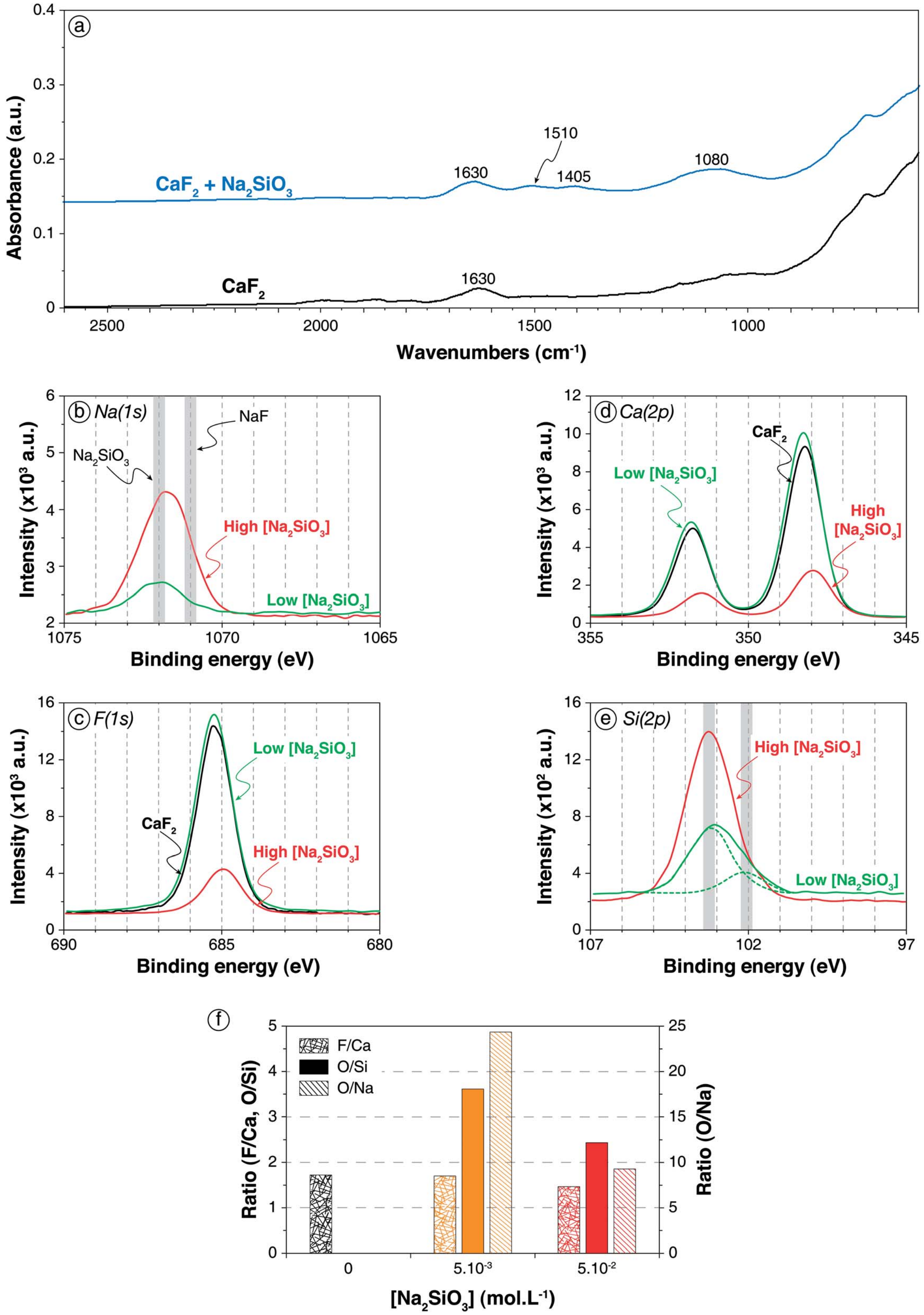

Fig. 2 Adsorption of Na_2SiO_3 onto CaF_2 surface. (a) Infrared spectra of CaF_2 conditioned in deionised water (black) and in a 5×10^{-2} mol L^{-1} Na_2SiO_3 solution (blue). (b) XPS Na(1s) spectra of CaF_2 conditioned in a 5×10^{-3} mol L^{-1} (green) and a 5×10^{-2} mol L^{-1} (red) Na_2SiO_3 solution, with the common binding energies of Na–O and Na–F bonds (from Moulder[62]). (c) XPS F(1s) spectra of CaF_2 conditioned in deionised water (black) and in 5×10^{-3} mol L^{-1} (green) and 5×10^{-2} mol L^{-1} (red) Na_2SiO_3 solutions. (d) XPS Ca(2p) spectra of CaF_2 conditioned in deionised water (black) and in 5×10^{-3} mol L^{-1} (green) and 5×10^{-2} mol L^{-1} (red) Na_2SiO_3 solutions. (e) XPS Si(2p) spectra of CaF_2 conditioned in a 5×10^{-3} mol L^{-1} (green) and a 5×10^{-2} mol L^{-1} (red) Na_2SiO_3 solution, with the common binding energies of SiO_2 and Si–O–X bonds.[56–58] (f) F/Ca, O/Si, and O/Na ratios of CaF_2 conditioned in deionised water (black), in a 5×10^{-3} mol L^{-1} Na_2SiO_3 solution (orange), and in a 5×10^{-2} mol L^{-1} Na_2SiO_3 solution (red). The ratios were calculated with the corresponding component for O and Si.

tetrahedra that induced a binding energy close to that of quartz.[62] Besides, the F/Ca ratio significantly decreased from 1.73 for pure CaF_2 to 1.47 for CaF_2 conditioned with high Na_2SiO_3 concentration (Fig. 2f). Since no calcium atoms were present in deionised water, this decrease was attributed to a surface depletion in terms of fluorine atoms. Considering the appearance of Ca–O bonds discussed previously, it could be considered that silica tetrahedra substituted fluorine atoms on the surface. The O/Si ratio was 2.45 (Fig. 2f), which indicated the adsorption of silica was in polymerised forms onto CaF_2. Also, the O/Na ratio was 9.30 which still indicated that protonated forms were dominant on the surface (Fig. 2f). The overall formula was $Si_{3.80}O_{9.30}NaH_{2.4}$, which corresponded to moderately polymerised silica in protonated and anionic forms.

To investigate the adsorption of Na_2SiO_3 as well as the increase of Na_2SiO_3 concentration, four different phenomena were studied by AIMD simulations: (1) the adsorption of monomeric protonated forms of silica, *i.e.* $Si(OH)_4$; (2) the adsorption of anionic forms of silica, *i.e.* $SiO(OH)_3^-$; (3) the increase of the surface coverage with protonated monomers; and (4) the adsorption of polymerised forms of silica, *i.e.* $Si_2O(OH)_6$.

(1) The lone molecule of $Si(OH)_4$ adsorbed in its molecular form with $\Delta E_{ads} = -100.7$ kJ mol^{-1} including $\Delta E_{disp} = -46.4$ kJ mol^{-1} (Fig. 3a and b), which confirmed the physisorption suggested by XPS results at low Na_2SiO_3 concentrations (Fig. 3c). Three oxygen atoms were bonded to three surface calcium atoms (Fig. 3b) with average Ca–O bond lengths of 2.65 Å, 2.78 Å, and 2.65 Å. The hydrogen atoms of the three –OH groups established H-bonds with surface fluorine atoms (Fig. 3b), the average lengths of which were all 1.66 Å.

(2) For the adsorption of $SiO(OH)_3^-$ form, a sodium atom was added on the surface near the $SiO(OH)_3^-$ molecule to keep the cell electrically neutral. During the simulation, the non-protonated oxygen atom ejected a fluorine atom from the surface and established three O–Ca bonds with three different surface calcium atoms, substituting a F^- in the upper fluorine atom layer (Fig. 3d). The ejected fluorine atom re-adsorbed onto a surface calcium atom and the sodium atom. Overall, the following reaction occurred:

$$\text{Surf–F} + \text{NaSiO(OH)}_3 = \text{Surf–SiO(OH)}_3 + \text{NaF} \quad (1)$$

The average distance between the non-protonated oxygen and the three surrounding calcium atoms was 2.54 Å. One protonated oxygen atom established an O–Ca and an O–Na bond with $d_{O–Ca} = 2.72$ Å and $d_{O–Na} = 2.27$ Å. The adsorption energy was $\Delta E_{ads} = -196.5$ kJ mol^{-1} including $\Delta E_{disp} = -56.9$ kJ mol^{-1}: the anionic form of silica tetrahedron, *i.e.* $SiO(OH)_3^-$, adsorbed with significantly higher energy in absolute value compared to the $Si(OH)_4$ form.

(3) To assess the influence of total silica concentration in solution, the surface coverage was successively increased to reach six $Si(OH)_4$ molecules, *i.e.* 100% coverage (Fig. 3a and e). From two to five molecules, the adsorption configuration was roughly the same as that with one $Si(OH)_4$ molecule, establishing however two Ca–O bonds instead of three. The molecules interacted with each other when they co-adsorbed, inducing a slight increase of adsorption energies in absolute values, from −100.7 kJ per mol per molecule for one molecule to −121.8 kJ per mol per molecule for five molecules (Fig. 3a). When added, the sixth molecule of $Si(OH)_4$ formed spontaneously $SiO(OH)_3^-$ and substituted a surface fluorine atom (Fig. 3e), which recombined with the proton to form HF on the surface:

$$\text{Surf–F} + 6\ \text{Si(OH)}_4 = \text{Surf–SiO(OH)}_3 + \text{HF} + 5\ \text{Si(OH)}_4 \quad (2)$$

This reaction, which induced an increase in absolute value of the adsorption energy to −131.1 kJ per mol per molecule, was in agreement with XPS results that demonstrated a depletion in fluorine atoms and the existence of Ca–O bonds when the Na_2SiO_3 concentration was high (Fig. 3c).

(4) $Si_2O(OH)_6$ adsorbed in its molecular form establishing four Ca–O bonds between four terminal (non-bonding) oxygen atoms and four different surface calcium atoms with $d_{O–Ca} = 2.53$ Å for three bonds and $d_{O–Ca} = 3.65$ Å for the fourth bond (Fig. 3f). Moreover, as for the $Si(OH)_4$ monomer, hydrogen atoms of the –OH groups established hydrogen bonds with surface fluorine atoms (Fig. 3b and f). Energetically speaking, the dimer adsorbed with $\Delta E_{ads} = -165.1$ kJ mol^{-1} including $\Delta E_{disp} = -70.4$ kJ mol^{-1}, which represented a significantly lower adsorption energy in absolute value compared to two monomers, regardless of their acid–base form.

3.2. Adsorption of Na_2SiO_3 on carbonated CaF_2 surface

The DRIFT spectrum of CaF_2 treated with 5×10^{-2} mol L^{-1} of Na_2CO_3 and 5×10^{-2} mol L^{-1} of Na_2SiO_3 sequentially is significantly different from the spectra of CaF_2 conditioned with each reagent alone (Fig. 4a). First, the bands located at 2492 cm^{-1} and at 1775 cm^{-1}, previously attributed to Na_2CO_3/$CaCO_3$, were no longer present when the two reagents were used together. Moreover, compared to CaF_2 conditioned with Na_2CO_3 only, the band at 879 cm^{-1}, ascribed to Na_2CO_3/$CaCO_3$, was significantly weaker while the band located at 842 cm^{-1}, attributed to $NaHCO_3$, exhibited a higher intensity (Fig. 4a). This indicated a higher amount of adsorbed $NaHCO_3$ when CaF_2 was conditioned with Na_2CO_3 + Na_2SiO_3. Also, CaF_2 conditioned only with Na_2CO_3 displayed one band at 1439 cm^{-1} and another at 1650 cm^{-1} while two peaks were present in each aforementioned zone for CaF_2 conditioned with Na_2CO_3 + Na_2SiO_3: two bands located at 1732 and 1667 cm^{-1} and two other bands at 1470 and 1383 cm^{-1} were exhibited (Fig. 4a), corresponding to both carbonate and hydrogencarbonate species. Furthermore, the band corresponding to Si–O asymmetric stretching vibration was narrower and shifted to 1057 cm^{-1} with a shoulder at 1023 cm^{-1} when CaF_2 was conditioned with Na_2CO_3 + Na_2SiO_3 (Fig. 4a). According to the literature, this could be attributed either to a higher amount of $SiO(OH)_3^-$ form rather than $Si(OH)_4$ form for silica tetrahedra or to a lower amount of polymerised silica on the surface.[23,65,66] Considering the higher amounts of $NaHCO_3$, it could be considered that one or both of the following reactions occurred on the surface:

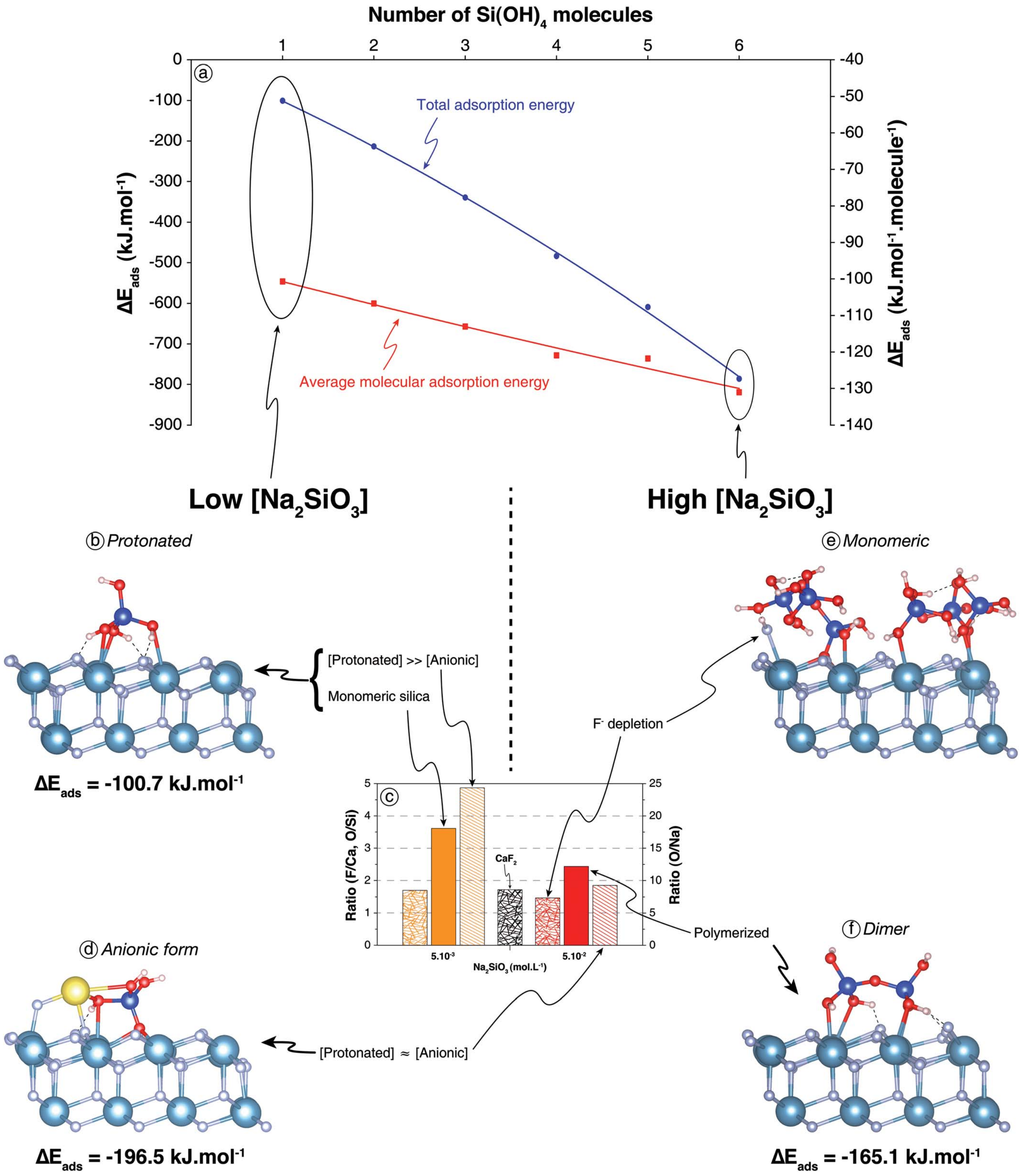

Fig. 3 (a) Total and molecular adsorption energies as a function of surface coverage for $Si(OH)_4$ molecules onto bare CaF_2 surface. (b) Snapshot of a side view of the (111) CaF_2 surface with a $Si(OH)_4$ molecule adsorbed after 50 ps of AIMD simulation. (c) F/Ca, O/Si, and O/Na ratios of CaF_2 conditioned in different conditions; refer to Fig. 2f for legends. (d) Snapshot of a side view of the (111) CaF_2 surface with a $NaSiO(OH)_3$ molecule adsorbed after 50 ps of AIMD simulation. (e) Snapshot of a side view of the (111) CaF_2 surface with six $Si(OH)_4$ molecules (100% coverage) adsorbed after 50 ps of AIMD simulation. (f) Snapshot of a side view of the (111) CaF_2 surface with a $Si_2O(OH)_6$ molecule adsorbed after 50 ps of AIMD simulation. The light blue, grey, red, dark blue, and yellow spheres represent calcium, fluorine, oxygen, silicon, and sodium atoms, respectively. Dashed lines represent hydrogen bonds.

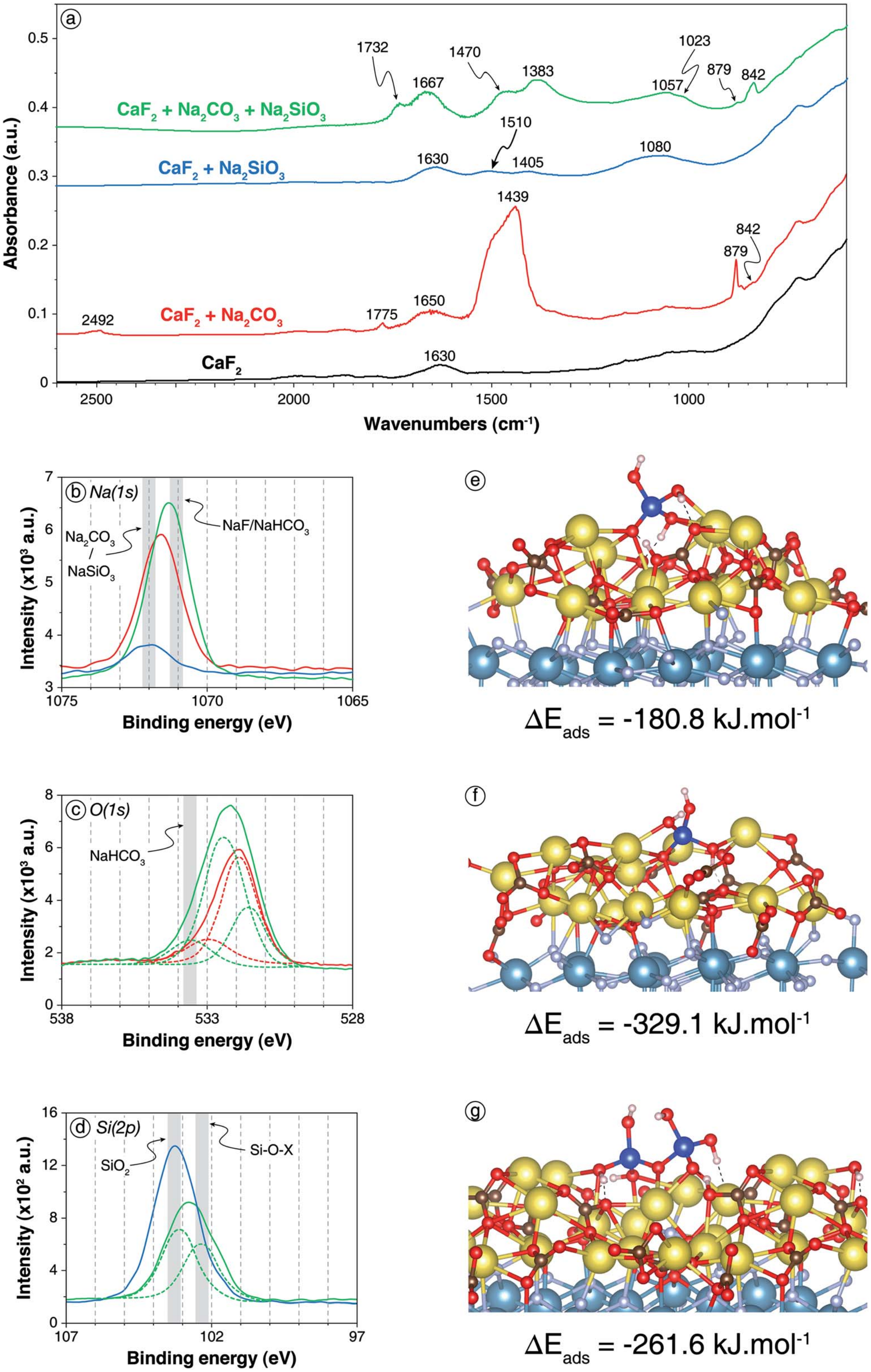

Fig. 4 Adsorption of Na_2SiO_3 onto carbonated CaF_2 surface. (a) Infrared spectra of CaF_2 conditioned in deionised water (black), in a 5×10^{-2} mol L^{-1} Na_2CO_3 solution (red), in a 5×10^{-2} mol L^{-1} Na_2SiO_3 solution (blue), and in a 5×10^{-2} mol L^{-1} Na_2CO_3 solution prior to in a 5×10^{-2} mol L^{-1} Na_2SiO_3 solution (green). (b) XPS Na(1s) spectra of the three last aforementioned samples (same colour scheme). (c) XPS O(1s) spectra of CaF_2 conditioned in a 5×10^{-2} mol L^{-1} Na_2CO_3 solution (red) and in a 5×10^{-2} mol L^{-1} Na_2CO_3 solution prior to in a 5×10^{-2} mol L^{-1} Na_2SiO_3 solution (green). d. XPS Si(2p) spectra of CaF_2 conditioned in a 5×10^{-3} mol L^{-1} Na_2SiO_3 solution (blue) and in a 5×10^{-3} mol L^{-1} Na_2CO_3 solution prior to in a 5×10^{-3} mol L^{-1} Na_2SiO_3 solution (green). (e) Snapshot of a side view of the carbonated (111) CaF_2 surface with a $Si(OH)_4$ molecule adsorbed onto the surface exhibiting a proton exchange. (f) Snapshot of a side view of the carbonated (111) CaF_2 surface with a $NaSiO(OH)_3$ molecule adsorbed onto the surface. (g) Snapshot of a side view of the carbonated (111) CaF_2 surface with a $Si_2O(OH)_6$ molecule adsorbed on the surface exhibiting a proton exchange. For colour scheme of spheres, refer to Fig. 1 and 2. Dashed lines represent hydrogen bonds.

$$Si(OH)_4 + CO_3^{2-} = SiO(OH)_3^- + HCO_3^- \quad (3)$$

$$Si_2O(OH)_6 + CO_3^{2-} + H_2O = SiO(OH)_3^- + Si(OH)_4 + HCO_3^- \quad (4)$$

in which the CO_3^{2-} ion is part of the Na_2CO_3 or $CaCO_3$ layer formed on the CaF_2 surface.

XPS analyses were also conducted on CaF_2 conditioned with low reagent concentrations, *i.e.* 5×10^{-3} mol L^{-1} for each, or with high reagent concentrations, *i.e.* 5×10^{-2} mol L^{-1}. For low reagent concentrations, sodium atoms were identified (5.0 at%) with Na(1s) binding energies of 1071.3 eV, which was significantly lower than the 1071.6 eV or 1071.9 eV displayed for CaF_2 + Na_2CO_3 and CaF_2 + Na_2SiO_3, respectively (Fig. 4b). This shift could be attributed to the formation of $NaHCO_3$ on the surface since this latter exhibits lower Na(1s) binding energy than Na_2CO_3.[62] Moreover, the peak at 533.6 eV exhibited in the O(1s) spectrum for CaF_2 + Na_2CO_3 + Na_2SiO_3, which was absent for CaF_2 + Na_2CO_3 and CaF_2 + Na_2SiO_3, corresponded to $NaHCO_3$.[71] The O/Si ratio was 4.03, which was slightly higher than the 3.61 exhibited for Na_2SiO_3 alone at the same concentration, indicating a possible depolymerisation of silica species on the surface induced by the carbonate layer.

When the reagent concentrations were increased to 5×10^{-2} mol L^{-1}, the surface chemical responses were very similar to those observed at low reagent concentrations. Interestingly, the Si(2p) spectrum displayed two components, at 103.1 eV (5.6 at%) and 102.3 eV (4.6 at%), while only one component at 103.2 eV was identified for CaF_2 + Na_2SiO_3 at the same concentration (Fig. 4d). Although the interpretation of Si(2p) spectra was difficult, the component at 103.1 eV was previously ascribed to Si–O–Si, *i.e.* polymerised silica, while the component at 102.3 eV was ascribed to Si–O–Na, *i.e.* non-polymerise and deprotonated silica.

To confirm these results, AIMD simulations were conducted on a carbonated surface. A complete layer of Na_2CO_3 was set on the (111) CaF_2 surface: a natrite supercell was created and fully relaxed at 0 K before generating the (110) surface, which presented crystallographic properties very close to those of the (111) fluorite surface. The natrite slab was then set on the (111) fluorite slab so that the CO_3^{2-} anions and the Na^+ cations corresponded spatially to Ca^{2+} cations and F^- anions, respectively. This carbonated surface was then used for the adsorption of Na_2SiO_3 at 300 K. As for bare CaF_2 surface, the adsorption of three different species was investigated: (1) the protonated monomer, *i.e.* $Si(OH)_4$; (2) the basic form of the monomer, *i.e.* $NaSiO(OH)_3$; and (3) the protonated form of the dimer, *i.e.* $Si_2O(OH)_6$.

The $Si(OH)_4$ molecule placed onto the carbonated (111) CaF_2 surface adsorbed establishing five Na–O bonds with two Na–O bonds formed by two different oxygen atoms and one Na–O bond by the last oxygen atom (Fig. 4e) with average bond lengths of between 2.36 and 2.88 Å. Each hydrogen atom established a hydrogen bond with an oxygen atom of the Na_2CO_3 layer. Besides, sometimes during the simulation, a proton was transferred from the $Si(OH)_4$ molecule to a CO_3^{2-} anion of the Na_2CO_3 surface layer (Fig. 4e). After a few picoseconds, it was transferred back to the $Si(OH)_4$, indicating that the two configurations coexisted on the surface with similar energy. This reaction on the surface was in good agreement with the formation of $NaHCO_3$ previously demonstrated by DRIFTS and XPS (Fig. 4a–d). Overall, $Si(OH)_4$ adsorbed onto the carbonated surface with $\Delta E_{ads} = -180.8$ kJ mol^{-1} including $\Delta E_{disp} = -45.0$ kJ mol^{-1} compared to $\Delta E_{ads} = -100.8$ kJ mol^{-1} including $\Delta E_{disp} = -46.4$ kJ mol^{-1} onto the bare surface.

The $NaSiO(OH)_3$ molecule placed onto the carbonated (111) CaF_2 surface adsorbed with the deprotonated oxygen atom establishing four Na–O bonds with average bond lengths of between 2.34 and 2.70 Å (Fig. 4f). Moreover, each protonated oxygen atom established one Na–O bond with the Na_2CO_3 layer with similar bond lengths. The hydrogen atoms formed hydrogen bonds with surface oxygen atoms while the sodium atom also adsorbed onto the Na_2CO_3 layer. Overall, the $NaSiO(OH)_3$ molecule adsorbed with $\Delta E_{ads} = -329.1$ kJ mol^{-1} including $\Delta E_{disp} = -73.7$ kJ mol^{-1}, which was significantly higher than for the bare surface.

The $Si_2O(OH)_6$ molecule set on the carbonated surface adsorbed with three non-bonding and the bonding oxygen atoms each establishing two Na–O bonds with average bond lengths of between 2.30 and 2.80 Å (Fig. 4g). Also, one proton

Table 2 Summary of the adsorption energies and surface reactions as a function of the surface coverage and the surface carbonation

Molecule	Number	Surface	ΔE_{ads} (kJ per mol per molecule)	ΔE_{disp} (kJ per mol per molecule)	Comments
$Si(OH)_4$	1	Bare	−100.7	−46.4	—
$Si(OH)_4$	6	Bare	−131.1	−49.4	Formation of HF by surface substitution of F^- by $SiO(OH)_3^-$
$NaSiO(OH)_3$	1	Bare	−196.5	−56.9	Formation of NaF by surface substitution of F^- by $SiO(OH)_3^-$
$Si_2O(OH)_6$	1	Bare	−165.1	−70.4	—
$Si(OH)_4$	1	Carbonated	−180.8	−45.0	Partial formation of $SiO(OH)_3^-$ by proton exchange with the surface
$NaSiO(OH)_3$	1	Carbonated	−329.1	−73.7	—
$Si_2O(OH)_6$	1	Carbonated	−261.6	−87.9	Formation of $Si_2O(OH)_5^-$ and partial formation of $Si_2O(OH)_4^{2-}$ by proton exchanges with the surface

was transferred durably from $Si_2O(OH)_6$ to a CO_3^{2-} anion of the surface, forming the $Si_2O_2(OH)_5^-$ species (Fig. 4g). Episodically during the simulation, a second proton was transferred between the adsorbed molecule and the surface, forming the $Si_2O_3(OH)_4^{2-}$ molecule. Overall, the dimer adsorbed with $\Delta E_{ads} = -261.6$ kJ mol^{-1} including $\Delta E_{disp} = -87.9$ kJ mol^{-1}, which represented significantly higher adsorption energies in absolute values compared to the bare surface.

XPS and DRIFTS results demonstrated that the prior treatment with Na_2CO_3 could induce a depolymerisation of silica on the surface. Hence, a $Si_2O(OH)_6$ molecule was set onto bare and carbonated surfaces along with an H_2O molecule, which is mandatory to enable the depolymerisation reaction. However, this reaction was not observed spontaneously.

Overall, based on the previous results, the following conclusions could be drawn, at pH 10:

(1) Conditioning with Na_2CO_3 induced the formation of a carbonate layer at CaF_2 surface.

(2) Na_2SiO_3 adsorbed on CaF_2 surface in both $Si(OH)_4$ and $SiO(OH)_3^-$ forms, with significant amount of polymerised forms of silica at the studied concentrations.

(3) The CO_3^{2-} ions contained in the surface carbonate layer accepted a proton from silica: $NaHCO_3$ was formed while deprotonated and/or depolymerised silica forms became dominant on the surface. The deprotonated forms of silica adsorbed better than the protonated forms, which could explain the synergistic effects observed between the two reagents.

3.3. Discussion

Considering the experimental and theoretical results, we demonstrated that the Na_2CO_3 layer formed on the surface induced a proton exchange between the silica molecules and the carbonated surface, even at low coverage (1 molecule, *i.e.* 16.7% coverage). This proton exchange occurred for the acid forms of the monomer [$Si(OH)_4$] and dimer [$Si_2O(OH)_6$], and, hence, probably for all the n-mers. This resulted in the formation of the basic, *i.e.* anionic, forms of these molecules, which adsorbed with significantly higher adsorption energies compared to their acid forms (Table 2). This proton exchange was observed for the bare surface only for high surface coverage (6 molecules, *i.e.* 100% coverage). These results explained the positive synergistic effects on the gangue minerals depression observed when the reagents are used in combination: the prior surface carbonation allows the formation of the anionic species of silica molecules by a surface acid–base reaction. It induces chemisorption of these molecules onto the surface for low coverage while a high coverage is needed to observe the same phenomenon on the bare surface. Increasing the solution pH would also lead to observation of the same phenomenon by increasing the amount of anionic silica species in solution. However, it would also result in hydroxylation of the surface cations, which would prevent the collector adsorption on all surfaces, including on the target mineral(s) surface.

4. Conclusion

In this article, we used a combination of surface spectroscopic methods (DRIFTS and XPS) and AIMD simulations to gain an understanding in the adsorption mechanisms of Na_2SiO_3 on fluorite, which represents an archetype of salt-type minerals. In particular, the synergistic effects observed when Na_2SiO_3 is used in combination with Na_2CO_3 in the froth flotation process were investigated. Both experimental and theoretical results demonstrated that Na_2CO_3 adsorbs onto fluorite and forms a carbonate layer on the surface. Also, they proved that $Si(OH)_4$, the most stable form of Na_2SiO_3 in dilute aqueous solutions at pH < 9.4, physisorbs with $\Delta E_{ads} = -100.7$ kJ mol^{-1} while $SiO(OH)_3^-$, stable for pH > 9.4, chemisorbs onto the surface by substituting a fluorine atom, with $\Delta E_{ads} = -196.5$ kJ mol^{-1}. The dimer $Si_2O(OH)_6$, representing polymerised forms stable for higher silica concentrations, physisorbs with $\Delta E_{ads} = -165.1$ kJ mol^{-1}, which is significantly lower than that for two monomers. The surface carbonation, induced by the prior addition of Na_2CO_3, leads to an acid–base reaction on the surface that results in the formation of the deprotonated forms of silica, regardless of the polymerisation degree, *i.e.* $SiO(OH)_3^-$, $Si_2O_2(OH)_5^-$, and $Si_2O_3(OH)_4^{2-}$. Also, experimental studies demonstrated that the surface carbonation leads to a silica depolymerisation on the surface. The anionic forms adsorbed with higher adsorption energies in absolute values compared to acid forms, as well as the monomers compared to the dimers. The formation of anionic forms on the bare surface needs either high silica coverage or high solution pH to be observed. Hence, at a moderate pH, a lower amount of Na_2SiO_3 is needed when the surface is carbonated to produce the same effect, explaining the strong synergistic effects highlighted when Na_2SiO_3 is used in combination with Na_2CO_3. Also, the deprotonation in solution by a pH increase would lead to hydroxylation of all the surfaces and then a global depression of all the minerals including the target mineral. This work allowed a gain in the understanding of the depressing effect of the combination of Na_2SiO_3 and Na_2CO_3 and could lead to a reduction of the Na_2SiO_3 amounts used worldwide in the flotation industry by using Na_2CO_3 instead of NaOH to control the pH.

Conflicts of interest

There are no conflicts to declare.

Acknowledgements

This work was granted access to the HPC resources of TGCC and CINES under the allocations 2018-A0050910306 and 2019-A0060910433 made by GENCI. The research leading to these results has received funding from the European Union's Horizon 2020 research and innovation programme under grant agreement no. 821265 for the FineFuture project. We also acknowledge the support of Labex Ressoures 21, supported by the French National Research Agency through the national programme "Investissements d'Avenir" with reference ANR-10-

LABX-21-LABEX RESSOURCES 21. Aurélien Renard, from the Laboratoire de Chimie Physique et Microbiologie pour les Matériaux et l'Environnement (UMR UL-CNRS 7564), is also acknowledged for the XPS analyses.

References

1 Markets and Markets, 2018.
2 A. Pedone, G. Malavasi, A. N. Cormack, U. Segre and M. C. Menziani, *Chem. Mater.*, 2007, **19**, 3144–3154.
3 T. Nakamura and M. Ogawa, *Langmuir*, 2012, **28**, 7505–7511.
4 P.-H. Chien, Y. Jee, C. Huang, R. Dervişoğlu, I. Hung, Z. Gan, K. Huang and Y.-Y. Hu, *Chem. Sci.*, 2016, **7**, 3667–3675.
5 K. M. Alotaibi, L. Shiels, L. Lacaze, T. A. Peshkur, P. Anderson, L. Machala, K. Critchley, S. V. Patwardhan and L. T. Gibson, *Chem. Sci.*, 2017, **8**, 567–576.
6 K. Baral, A. Li and W.-Y. Ching, *J. Phys. Chem. A*, 2017, **121**, 7697–7708.
7 G. Lagaly, W. Tufar, A. Minihan and A. Lovell, in *Ullmann's Encyclopedia of Industrial Chemistry*, Wiley-VCH Verlag GmbH & Co. KGaA, Wiley-VCH Verlag GmbH & Co. KGaA, Weinheim, Germany, 2000.
8 V. Kahlenberg, *CHIMIA International Journal for Chemistry*, 2010, **64**, 716–722.
9 J. E. Shelby, *Introduction to glass science and technology*, Royal Society of Chemistry, Cambridge, 2nd edn, 2005.
10 J. Swenson and S. Adams, *Phys. Rev. Lett.*, 2003, **90**, 155507.
11 L. O. Filippov, Q. Dehaine and I. V. Filippova, *Miner. Eng.*, 2016, **95**, 96–106.
12 M. Ejtemaei, M. Irannajad and M. Gharabaghi, *Int. J. Miner. Process.*, 2012, **114–117**, 40–47.
13 D. S. Rao, T. V. VijayaKumar, S. S. Rao, S. Prabhakar and G. B. Raju, *Int. J. Miner., Metall. Mater.*, 2011, **18**, 515–522.
14 L. O. Filippov, Y. Foucaud, I. V. Filippova and M. Badawi, *Miner. Eng.*, 2018, **123**, 85–94.
15 N. Kupka and M. Rudolph, *Int. J. Min. Sci. Technol.*, 2018, **28**, 373–384.
16 X. Yang, *Miner. Eng.*, 2018, **125**, 111–119.
17 Y. Foucaud, I. V. Filippova and L. O. Filippov, *Powder Technol.*, 2019, **352**, 501–512.
18 S. Song, A. Lopez-Valdivieso, C. Martinez-Martinez and R. Torres-Armenta, *Miner. Eng.*, 2006, **19**, 912–917.
19 W. Zhou, J. Moreno, R. Torres, H. Valle and S. Song, *Miner. Eng.*, 2013, **45**, 142–145.
20 H. Sis and S. Chander, *Miner. Eng.*, 2003, **16**, 577–585.
21 G. W. Qi, C. Klauber and L. J. Warren, *Int. J. Miner. Process.*, 1993, **39**, 251–273.
22 I. Halasz, M. Agarwal, R. Li and N. Miller, *Catal. Lett.*, 2007, **117**, 34–42.
23 J. L. Bass and G. L. Turner, *J. Phys. Chem. B*, 1997, **101**, 10638–10644.
24 K. I. Marinakis and H. L. Shergold, *Int. J. Miner. Process.*, 1985, **14**, 177–193.
25 C. W. Lentz, *Inorg. Chem.*, 1964, **3**, 574–579.
26 D. Dimas, I. Giannopoulou and D. Panias, *J. Mater. Sci.*, 2009, **44**, 3719–3730.
27 J. Nordström, E. Nilsson, P. Jarvol, M. Nayeri, A. Palmqvist, J. Bergenholtz and A. Matic, *J. Colloid Interface Sci.*, 2011, **356**, 37–45.
28 K. I. Marinakis, 1980.
29 Y. Han, W. Liu and J. Chen, *Appl. Surf. Sci.*, 2016, **370**, 403–409.
30 P. S. Roller and G. Ervin, *J. Am. Chem. Soc.*, 1940, **62**, 461–471.
31 4, 488, 959, 1984, 17.
32 E. Potapova, M. Grahn, A. Holmgren and J. Hedlund, *J. Colloid Interface Sci.*, 2010, **345**, 96–102.
33 N. V. Tran, A. K. Tieu, H. Zhu, H. T. T. Ta, T. D. Ta and H. M. Le, *J. Phys. Chem. C*, 2018, **122**, 20827–20840.
34 D. Azizi and F. Larachi, *Colloids Surf., A*, 2018, **537**, 126–138.
35 B. S. Shin and K. S. Choi, *Mining, Metallurgy & Exploration*, 1985, **2**, 223–226.
36 N. Kupka and M. Rudolph, *Miner. Eng.*, 2018, **129**, 120–128.
37 T. Ogawa, T. Aonuma, T. Tamaki, H. Ohashi, H. Ushiyama, K. Yamashita and T. Yamaguchi, *Chem. Sci.*, 2014, **5**, 4878–4887.
38 X. Li, Z.-J. Zhao, L. Zeng, J. Zhao, H. Tian, S. Chen, K. Li, S. Sang and J. Gong, *Chem. Sci.*, 2018, **9**, 3426–3437.
39 X. Liu, Y. Tang, M. Shen, W. Li, S. Chu, B. Shan and R. Chen, *Chem. Sci.*, 2018, **9**, 2469–2473.
40 P. Zhou, X. Hou, Y. Chao, W. Yang, W. Zhang, Z. Mu, J. Lai, F. Lv, K. Yang, Y. Liu, J. Li, J. Ma, J. Luo and S. Guo, *Chem. Sci.*, 2019, **10**, 5898–5905.
41 I. Píš, E. Magnano, S. Nappini and F. Bondino, *Chem. Sci.*, 2019, **10**, 1857–1865.
42 G. Lovat, E. A. Doud, D. Lu, G. Kladnik, M. S. Inkpen, M. L. Steigerwald, D. Cvetko, M. S. Hybertsen, A. Morgante, X. Roy and L. Venkataraman, *Chem. Sci.*, 2019, **10**, 930–935.
43 C. Shen, I. Cebula, C. Brown, J. Zhao, M. Zharnikov and M. Buck, *Chem. Sci.*, 2012, **3**, 1858.
44 H. H. Kristoffersen, T. Vegge and H. A. Hansen, *Chem. Sci.*, 2018, **9**, 6912–6921.
45 Y. Foucaud, S. Lebègue, L. O. Filippov, I. V. Filippova and M. Badawi, *J. Phys. Chem. B*, 2018, **122**, 12403–12410.
46 Y. Foucaud, M. Badawi, L. Filippov, I. Filippova and S. Lebègue, *Miner. Eng.*, 2019, **143**, 106020.
47 T. C. Parks and W. W. Barker, *J. Solid State Chem.*, 1977, **20**, 397–407.
48 P. W. Tasker, *Le Journal de Physique Colloques*, 1980, **41**, C6–C488.
49 N. H. de Leeuw, J. A. Purton, S. C. Parker, G. W. Watson and G. Kresse, *Surf. Sci.*, 2000, **452**, 9–19.
50 P. Hohenberg and W. Kohn, *Phys. Rev.*, 1964, **136**, B864–B871.
51 W. Kohn and L. J. Sham, *Phys. Rev.*, 1965, **140**, A1133–A1138.
52 G. Kresse and J. Hafner, *Phys. Rev. B: Condens. Matter Mater. Phys.*, 1993, **47**, 558–561.
53 J. P. Perdew, K. Burke and M. Ernzerhof, *Phys. Rev. Lett.*, 1996, **77**, 3865–3868.
54 P. E. Blöchl, *Phys. Rev. B: Condens. Matter Mater. Phys.*, 1994, **50**, 17953–17979.
55 G. Kresse and D. Joubert, *Phys. Rev. B: Condens. Matter Mater. Phys.*, 1999, **59**, 1758–1775.

56 G. Kresse and J. Furthmüller, *Phys. Rev. B: Condens. Matter Mater. Phys.*, 1996, **54**, 11169–11186.

57 M. Methfessel and A. T. Paxton, *Phys. Rev. B: Condens. Matter Mater. Phys.*, 1989, **40**, 3616–3621.

58 S. Grimme, *J. Comput. Chem.*, 2006, **27**, 1787–1799.

59 F. A. Miller and C. H. Wilkins, *Anal. Chem.*, 1952, **24**, 1253–1294.

60 M. Roche, *Caractérisation de l'état de surface des fluorines et application à la flottation des minerais de fluorine du district du Tarn (Montroc - Le Burc)*, PhD thesis, Université de Nancy I, 1973.

61 K. I. Marinakis and H. L. Shergold, *Int. J. Miner. Process.*, 1985, **14**, 161–176.

62 J. F. Moulder, *Handbook of X-ray photoelectron spectroscopy: a reference book of standard spectra for identification and interpretation of XPS data*, Perkin-Elmer Corporation, Eden Prairie, Minn, Update, 1992.

63 Y. Foucaud, M. Badawi, L. O. Filippov, I. V. Filippova and S. Lebègue, *J. Phys. Chem. B*, 2018, **122**, 6829–6836.

64 Y. Foucaud, M. Badawi and L. Filippov, *Miner. Eng.*, 2019, **135**, 156–159.

65 H. Jansson, D. Bernin and K. Ramser, *AIP Adv.*, 2015, **5**, 067167.

66 R. Gaggiano, I. De Graeve, J. M. C. Mol, K. Verbeken, L. A. I. Kestens and H. Terryn, *Surf. Interface Anal.*, 2013, **45**, 1098–1104.

67 E. Merlen, J. Lynch, M. Bisiaux and F. Raatz, *Surf. Interface Anal.*, 1990, **16**, 364–368.

68 T. L. Barr, *J. Phys. Chem.*, 1978, **82**, 1801–1810.

69 S. Carniato, J.-J. Gallet, F. Rochet, G. Dufour, F. Bournel, S. Rangan, A. Verdini and L. Floreano, *Phys. Rev. B: Condens. Matter Mater. Phys.*, 2007, **76**, 085321.

70 L. Pauling, *The nature of the chemical bond and the structure of molecules and crystals: an introduction to modern structural chemistry*, Cornell Univ. Press, Ithaca, New York, 3rd edn, 17 print, 2000.

71 A. Shchukarev and D. Korolkov, *Cent. Eur. J. Chem.*, 2004, **2**, 347–362.